Numerical simulation of full-scale steel-frame undergoing soil pressure

Bayang Zhang

Key Laboratory of Impact and Safety Engineering Ministry of Education,
Ningbo University,
Ningbo, Zhejiang 315211, China
Email: 864373098@qq.com

Yaohong Zhu

Collaborative Innovation Centre of Coastal Urban Rail Transit,
Ningbo University,
Ningbo, Zhejiang 315211, China
and
Ningbo Rail Transit Group Co., Ltd.,
Ningbo, Zhejiang 315211, China
Email: zhuyaohong@nbu.edu.cn

Fachao Li, Jiawei Wang and Jue Zhu*

Key Laboratory of Impact and Safety Engineering Ministry of Education,
Ningbo University,
Ningbo, Zhejiang 315211, China
Email: 1094532412@qq.com
Email: 4ka8@sina.com
Email: zhujue@nbu.edu.cn
*Corresponding author

Abstract: During the excavation of connecting channel between the main tunnels using the mechanical shield method or pipe jacking method, the loading situation on the T-joint is very complicated. A vertical loaded full-scale steel-frame which can imitate the surrounding soil loading is invented to ascertain the action mechanism of each part. It can burden seven-ring segments and concern the soil spring effect. Prior to the field test, the entire installation of the facility is modelled, simulated and analysed to evaluate the safety of the construction. The analysis results show that the steel frame rotates seriously when the steel frame is not welded to the base. After welding the steel frame with the base, the rotation phenomenon of the steel frame can be effectively eliminated and the stress and displacement of each part are in line with the standard for design of steel structures.

Keywords: steel frame; vertical loaded; soil spring; earth pressure; seven-ring.

Reference to this paper should be made as follows: Zhang, B., Zhu, Y., Li, F., Wang, J. and Zhu, J. (2022) 'Numerical simulation of full-scale steel-frame undergoing soil pressure', *Int. J. Computer Applications in Technology*, Vol. 68, No. 1, pp.27–38.

Biographical notes: Bayang Zhang is a graduate student at Ningbo University. His research interests include numerical simulation, corrosion and protection of biomass carbonization kettle.

Yaohong Zhu is a Bridge and Underground Engineering Expert, Professor of Ningbo University, Chief Engineer of Ningbo Rail Transit Group Co., Ltd. He is well known in the field of bridge and underground engineering.

Fachao Li is a graduate student at Ningbo University. His research focuses on dynamic instability of Z-section cold-formed steel members under axial impact

Jiawei Wang is a graduate student at Ningbo University. His research interests include constitutive equation of G550 steel in high-temperature and high-strain rate condition.

Jue Zhu received her PhD degree from the University of Science and Technology of China in 2006. Now, she is a Professor at the Faculty of Mechanical Engineering and Mechanics, Ningbo University. Her research interests include the static and dynamic stability of cold-formed steel structures and the durability of seawater eroded concrete.

1 Introduction

Urban traffic flow in China has increased significantly in recent years. As a safe, fast, efficient and environment friendly form of transportation, the metro has become the primary choice for many large cities to relieve traffic pressure.

The mechanical shield method has been developed and used for many years and given a lot of feasible experience in metro facilities (Aso et al., 1995). In the construction of Ningbo Rail Transit, this method is firstly used to excavate the connecting channel between the main tunnels. The structural stability of T-joint between the main tunnel and connecting channel during the excavation is the most important factor should to be considered.

Many studies have been carried out on the structural performance of T-joint by using scaling or full-scale experimental models to examine the complex interaction between the T-joint and its surrounding soil (Li et al., 2015).

In 2003, Tongji University established a set of loading equipment to imitate the transversal water and earth pressure on 1:1 double-circle staggered assembling lining (Guo et al., 2004), as shown in Figure 1. Multi-point equivalent loading by jacks, instead of actually distributional loading, is imposed to the periphery of the rings.

Figure 1 Double circle lining single ring test (Guo et al., 2004)

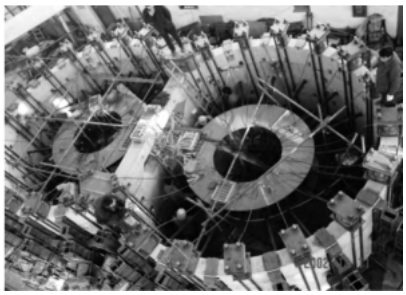

Fang et al. (2016) designed an experimental model with a geometric ratio of 1:10, a density ratio of 1:1, and a hydraulic loading device to simulate the effect of real water pressure on shield tunnel, as shown in Figure 2. Horizontal jacks were arrayed to impose the loading on the horizontal samples. A series of steel strands were used to induce the uniform water pressure to the periphery of ring segments. Further, by controlling the tensile angle and force, non-uniform water pressure was imitated.

Owing to the large friction force generated by the ground surface, the above horizontal model is unable to imitate the rotational deformation around the longitudinal axis and the influence of the structural self-weight. It failed to achieve the structural integrity conducted by mechanical loading test of segment and joint. In order to imitate the mechanical behaviour of shield lining structure under actual stress and explore the influence of the deformations of segment and joint caused by self-weight of the structure. At Tongji University, Liu et al. (2017) established a 1:1 prototype three-ring vertical loading device, including the reaction frame and spring support group. They proposed the loading method of hydraulic control system of jacks based on PLC closed loop control theory, as shown in Figure 3. By analysing the distribution of cracks on the inner and outer cambered surfaces of the pipe segment, it was found that the bending moment transfer phenomenon of the special-shaped pipe segment is obvious.

Figure 2 Tunnel horizontal loading test platform (Fang et al., 2016)

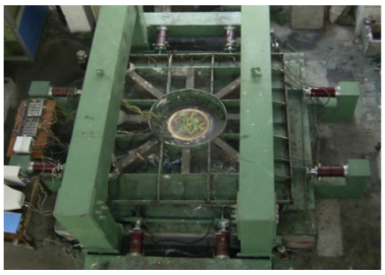

Figure 3 Vertical loading test device (Liu et al., 2017)

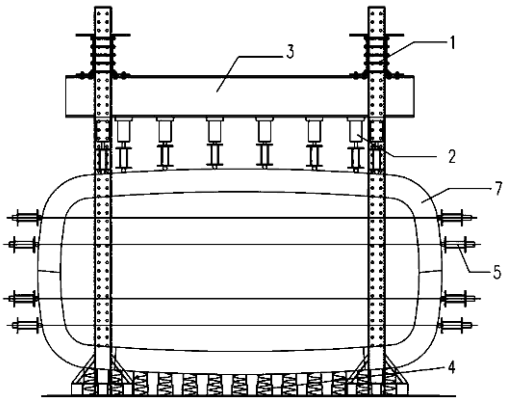

Based on the segment bending moment transmission discovered by Tongji University, it is necessary to expand the research from the original three rings to seven rings to comprehensively imitate the real stress situation in the experimental excavation of connecting channel with the mechanical shield method. This article introduces a comprehensive seven-ring test platform for researching the mechanical properties, as shown in Figure 4. The test platform is a reaction frame being composed of seven-ring full-scale steel ring frame. Each ring consists of 24 jacks. The displacement control accuracy of the jack is 0.1 mm. It can simulate soil loads up to 30 m deep or 150 tons soil weight. The whole set is 10.08 m high, which can be applied to the

lining ring loading test with outer diameter of 6.0–6.8 m and width of 1.2–1.5 m.

Figure 4 Seven-ring test platform

Owing to the long period and high cost of practical engineering experiments, some scholars use numerical simulation technology (Jiwattanakul et al., 2021; Sayahi et al., 2021) to carry out related research and analysis. Ma (2015) imitated the actual loads of the tunnel in the formation by SPA2000 finite element software. Considering the conventional water and earth pressure in the experiment, other factors such as elastic resistance of ground, overcharge on ground, and complex distributed loads are also taken into account, so that the bearing capacity and deformation characteristic of the tunnel segments can be more realistically understood. Ding et al. (2004) proposed a two-dimensional finite element model considered the four stages during construction. The characteristics of the surrounding soil material are assumed to be elastoplastic. According to the contact state between the soil and the lining, the stress coefficient is used to study the process of construction changes, and the model's results are compared with the site of the No. 7 subway in Osaka, Japan. The corresponding results show that the model can effectively estimate the deformation of surrounding soil and concrete lining sections. Based on the characteristics of shield tunnel construction in sections, grouting materials and segments joint, Zhu (1999) proposed different finite elements simulation techniques, and applied it to the construction of the shield tunnel of Osaka No. 7 subway line. Compared with the measured data, the analysis results show that the calculated data under the non-uniform conditions is closer to measured data then under uniform conditions.

Using the finite element software, the full-scale steel-frame model was simulated and analysed to find the dangerous section and safety hazard, and the improvement of the foundational restraint of the experimental steel frame was put forward. This can provide reference and guidance for practical engineering.

2 Experimental facility

The comprehensive test platform of seven-ring shield tunnel shown in Figure 5.

It includes eight parts: 1) Modular earth pressure imitation apparatus; 2) Modular support base; 3) Formation imitation device and segment clamping apparatus; 4) Loading imitation apparatus of longitudinal residual force; 5) Unit assembly and transport device; 6) Unit lifting apparatus; 7) Shield machine receiving device and 8) Foundation base.

Figure 5 Full-scale comprehensive experimental platform

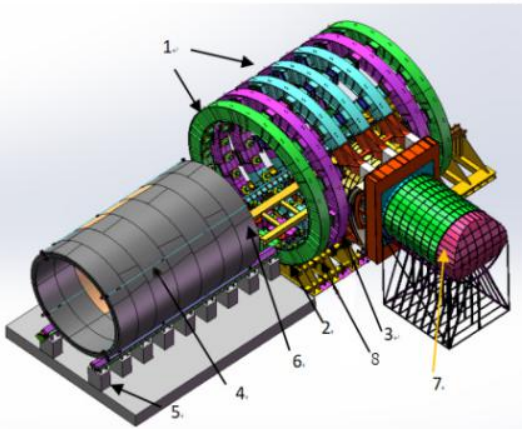

The platform can carry out the following experiments:

1) It can realistically imitate the detailed characteristics of the segment lining structure under normal loading and ultimate loading conditions, as well as the mechanical properties such as structural bearing capacity, instability and failure mechanism and force transfer between the rings.

2) It can effectively explore the influence of excavating the main tunnel segment on itself and the adjacent ring segments during the T-joint construction process.

3) An intelligent control system is integrated to imitate the effect of 'soil spring'.

The control system has three loading control methods (loading control method, displacement control method and loading-displacement control method) to realise the imitation under various working conditions. In the loading control method, it drives the hydraulic jack to the rated load, which is used to imitate the 'soil column theory' and calculate the water and earth pressure at the top. Displacement control method drives the jack to a set of displacement values. It is used to imitate sub-grade contact pressure under the condition of constant displacement, which can also passively generate the corresponding load. The third control method is called load-displacement control method, it is to calculate the load-displacement curve of the jack according to the foundation soil coefficient of sub-grade reaction and then determine the corresponding load values by the jack displacement control. The waist jacks adopt this load-displacement control method to imitate the passive earth pressure. The whole loading device imitates each stage under various working conditions by means of hierarchical loading and unloading.

There are 168 sets of jack loading devices applied to load and unload the specimen, with 24 loading points per ring (shown in Figures 6 and 7) evenly distributed on the external surface of the special seven-ring concrete-steel composite

segments. P1 is mainly used to simulate the water and soil pressure at the top of the tunnel, P2 is used to simulate the lateral water and soil pressure of the tunnel and P3 is used to simulate the water and soil pressure at the transition section of the tunnel shoulder. The hydraulic loading system is used to imitate the ground resistance, water and soil pressure and ground overload of the actual shield tunnel structure through the horizontal concentrated load of 24 points.

Figure 6 Schematic diagram of 24-point loading of the experimental frame

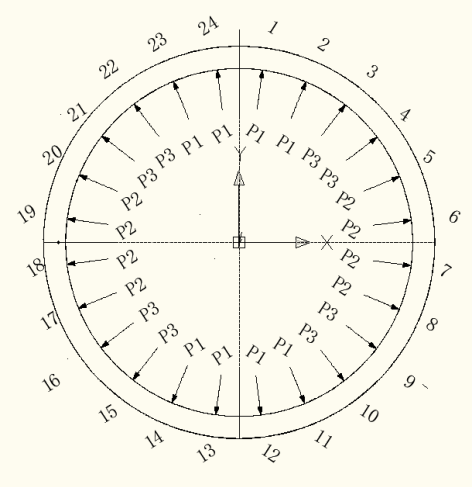

3 Finite element simulation

3.1 Model establishment

Before the propulsion of shield machine, numerical simulation was conducted to predict the safety of the steel frame.

The refined experimental model of full-scale steel-frame is established, and then exported into Hypermesh and Abaqus for pre-processing and analysis. The 3-D model is shown in Figure 7. In model, the units of length, mass, time are set as mm, ton and sec.

Figure 7 Full-scale steel frame model

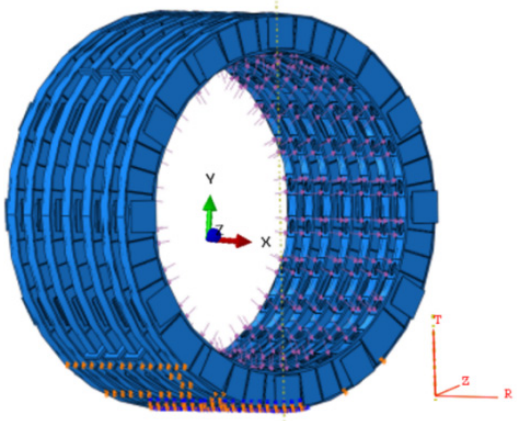

The steel frame is made of Q345 steel with density of ρ=7.83×10^{-9}t/mm^3, elastic model E=2.08×10^{5}MPa, Poisson's ratio is 0.28 and yield strength is 345 MPa. High strength bolts, class 10.9, are used for connection between adjacent rings and segments. The yield strength ratio of the bolt material is 0.9, that is, the nominal yield strength is 900 MPa, the nominal tensile strength is 1000 MPa.

The following contacts will be defined in the finite element model: merge is used between rings of steel frame. Face to face contact is adopted between bolt and steel frame. The quadratic tetrahedral elements of type C3D10 are applied to divide the model. The minimum size of the dividing element is 6.3 mm. The approximate global size is adopted for mesh generation, and its size is 150 mm.

The cylindrical coordinates are set as shown in Figure 7. R, T and Z, respectively mean radial, circumferential and axial directions and their displacements are U1, U2 and U3. At both ends of the model, only the value of U1 is set as 0, which means the radial displacement of the steel frame is restricted.

3.2 Analysis procedures

Considering the different external loading, the following six working conditions are listed.

1) *Design condition*: It refers to the load distribution when the surrounding environment is not excavated and only subjected to water and earth pressure.
2) *Unloading condition*: It considers the eccentric load distribution on the ring due to the lateral soil is excavated in the process of construction.
3) *Overload condition*: It describes the case where the above-ground loading changes greatly or the new structure constructed nearby. It is characterised by long-term action on the tunnel and must be evaluated as a load condition.
4) 4–6) *Three special loading conditions*: They are called special working conditions that refer to the special situations where the connecting channel has been excavated through.

The test design adopts deep buried segment reinforcement, and the buried depth is calculated at 17 m. According to the principle of symmetry, the 24 loading points were divided into 3 groups (shown in Figure 6). The magnitude of the concentrated forces P1, P2 and P3 are converted by the uniform forces acting on the lining ring, and adjusted based on the principle that the structural deformation and the internal forces of the control section are equivalent under the actual operation and test conditions, so as to ensure that the errors of the structural deformation and the internal forces of the control interface are within a certain range. The load value of each loading point in the same group is the same, and the load value of each jack in the same loading point is the same, which is completely synchronised during loading. After calculation, the summary of operating conditions P1, P2 and P3 is shown in Table 1.

In the tests on site, loadings are changed by the deformation of the rings automatically based on site conditions. It will be discussed in Section 4.

Table 1 Loading conditions

Serial number	*Working condition*	*P1(kN)*	*P2(kN)*	*P3(kN)*
1	Design condition	382.00	243.00	298.00
2	Unloading condition	467.62	169.78	274.10
3	Overload condition	970.00	626.00	766.00
4	Special design conditions	382.00	*P*2=0 on the excavating side	298.00
5	Special unloading conditions	467.62	*P*2=0 on the excavating side	274.10
6	Special overload condition	970.00	*P*2=0 on the excavating side	766.00

3.3 Simulational results

As shown in Table 2, if the steel frame isn't constrained except for radial direction, the circumferential rotational displacement, 4.74×10^3 mm, has greatly exceeded the jack's allowable displacement, viz., it should not be larger than 5mm. It will affect the accuracy of loading, furthermore, directly cause the collapse of whole steel frame. This kind of circumferential rotation tendency has not been reported in previous horizontal-laid model experiments and it is a particular situation encountered in the vertical loading steel frame.

Table 2 Seven ring steel frame simulation result

Seven ring steel frame	σ_{max} *MPa*	τ_{12max} *MPa*	U_{1max} *mm*	U_{2max} *mm*	U_{3max} *mm*
Three loads	128.9	53.6	4.74×10^3	4.74×10^3	0.41

In order to investigate the cause of the rotation, the middle ring of the steel frame is taken for analysis. The former three working conditions shown in Table 1 are considered, huge circumferential rotation deformations, respectively, 27.69 mm, 28.20 mm and 90.76 mm, are still occurred on the steel frame model, as shown in Table 3.

Table 3 Displacement results of ring without welding under different working conditions

Working condition	*Maximum stress (MPa)*	*Maximum total displacement (mm)*	*Maximum circumferential displacement (mm)*
Design condition	72.98	37.60	27.69
Unloading condition	107.50	31.35	28.20
Overload condition	184.30	96.80	90.76

It has been found that the connecting bolts are subjected to shear failure due to great circumferential displacement. In order to confirm that the great circumferential displacement is caused by the asymmetry of the model, the elastic modulus of the steel is increased by 100 times, viz. setting elastic modulus as 2.08×10^7 MPa. In the model, the friction between steel frame and foundation base is considered, in which the friction coefficient is set as 0.15. Finally, the special seven-ring steel-concrete composite ring barely rotates. Under the design condition, the circumferential deformation nephogram is shown in Figure 8.

The maximum total displacement and maximum circumferential displacement of the model under design conditions is approximately 1/100 of the former ones, which implies that the circumferential rotation is caused by the tangential moment generated by the inner uncoordinated deformation of the steel frame. So a fixed constraint between steel frame and foundation base is proposed.

After comprehensive consideration, within the region of arc length of 1m between frame and base, the frame is welded to the base, as shown in Figure 9, the contact between them is set as fixed. This modification successfully prevents the circumferential displacement of the steel frame under three working conditions. The analysis results after welded are displayed in the next subsection.

Figure 8 Circumferential displacement diagram of the middle ring

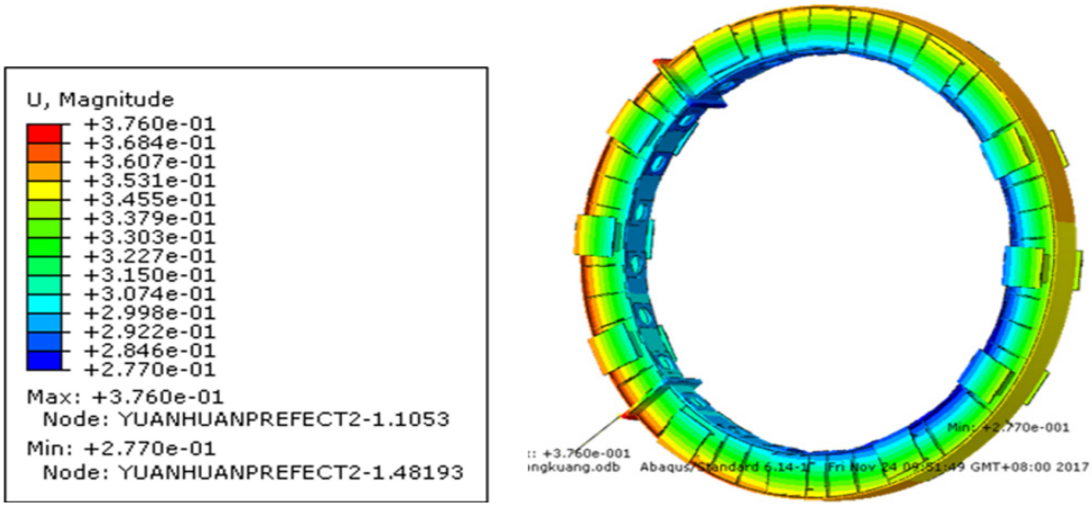

Figure 9 Schematic diagram of loading constraints

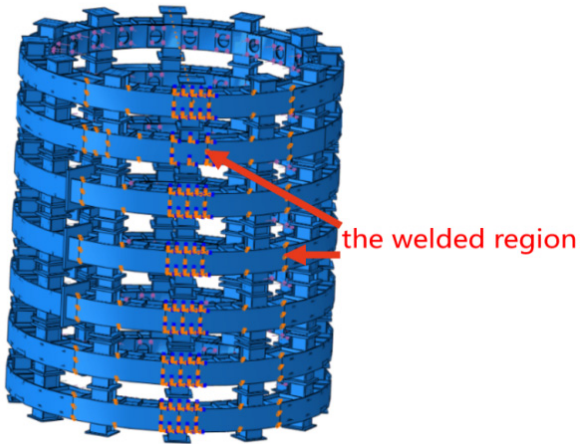

3.4 Simulational results after welded

The nephograms of Mises stress, shear stress and displacement under special overloading working conditions are shown in Figures 10 to 13.

The maximum Mises stresses and shears respectively exist in the jacks assemble plate Figure 10 and the rightmost web of the steel frame Figure 11. The U2max means a counterclockwise rotation trend in the whole steel frame. Circumferential constraints (U1+U2+U3) are carried out on both sides (1m*1cm) of the base to simulate the weld. Under the most dangerous special overload condition, the maximum shear stress of a weld is 678.9 kN. Each ring weighs 29 tons and the friction provided by the base cannot stop its rotation. Therefore, a large rotation trend appears in Figure 13, and the corresponding value reaches 8.8 mm.

Figure 10 Nephogram of Mises stress in special overloading condition (MPa)

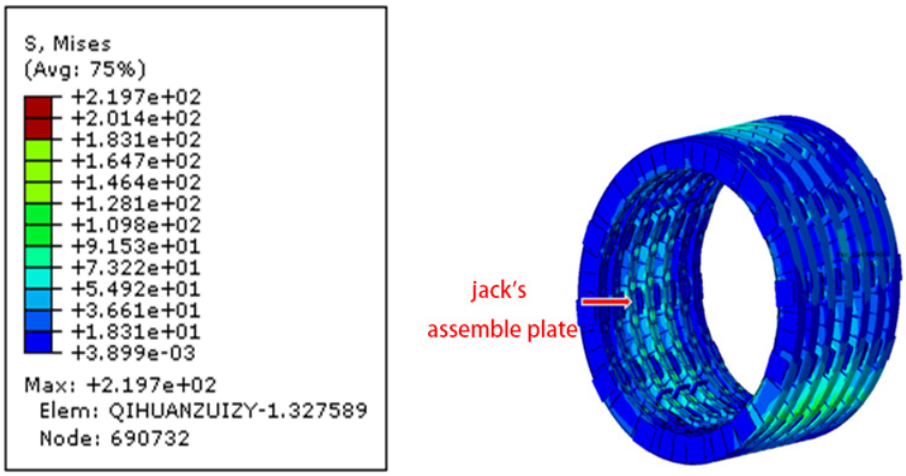

Figure 11 Nephogram of shear stress in special overloading condition (MPa)

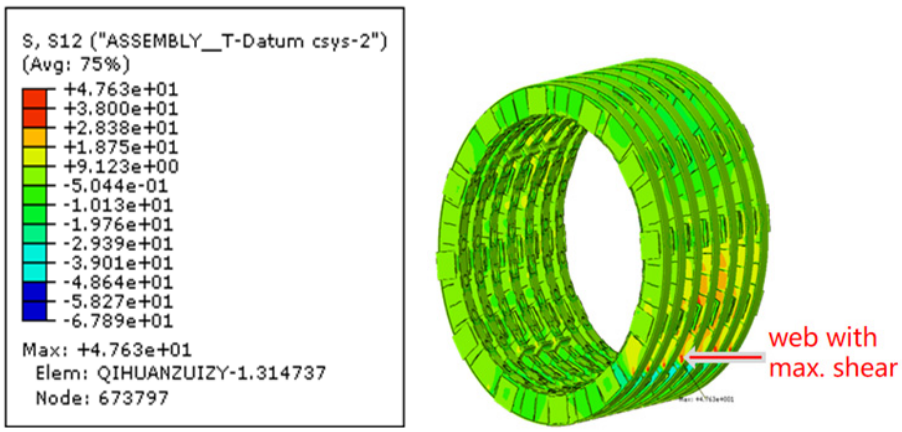

Figure 12 Displacement distribution nephogram (U1) in special overloading condition (mm)

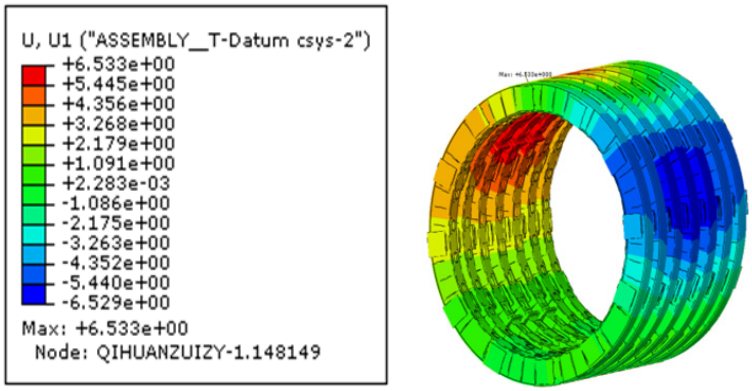

Figure 13 Displacement distribution nephogram (U2) in special overloading condition (mm)

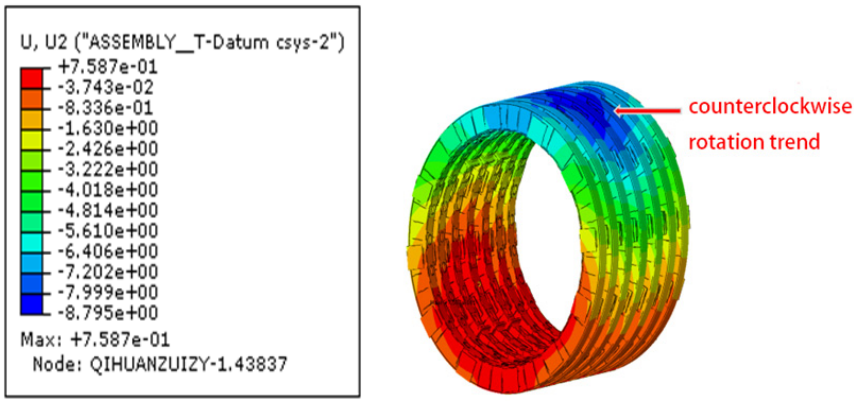

The summary of maximum values under six working conditions is listed in Table 4. In Standard for design of steel structures of the China GB 50017-2017 (GB, 2017). The design strength resistant and weld resistant of steel Q345 are shown in Table 5. From the two tables, it can be seen that the design strength of the steel frame after welded with the foundation base can meet the design requirements.

Table 4 Summary of various working conditions data

Working conditions	σ_{max} *MPa*	τ_{12max} *MPa*	$\tau_{12max\ (Longitudinal)}$ *MPa*	U_{1max} *mm*	U_{2max} *mm*
Design condition	126.7	25.72	10.0	1.67	0.93
Unload condition	65.61	20.87	12.53	2.00	1.14
Overload condition	188.8	59.45	18.39	3.06	1.60
Special design condition	126.2	27.25	16.68	2.81	0.36
Special unload condition	92.6	23.16	15.00	2.72	3.02
Special overload condition	219.7	67.89	35.00	6.53	8.80

Note: (τ12max (Longitudinal) abbreviation of the maximum shear stress at the longitudinal connection plate.

Table 5 Design resistant and design weld resistant of steel Q345 (GB, 2017)

Q345 steel Thickness or diameter (mm)	*Tensile, bending and compression resistant (MPa)*	*Shear resistant (MPa)*	*Weld strength Tensile and compression resistant (MPa)*	*Weld strength shear resistant (MPa)*
≦16	310	175	305	175
16–40	295	170	295	170
40–63	290	165	290	165
63–80	280	160	280	160

Note: the butt weld quality is first grade.

The radial and circumferential displacement in three special working conditions are larger. U2max, appearing in the upper right position of the middle ring, is 8.80 mm. The jack will break due to the excessive displacement of the circumferential direction. Therefore, the stiffness of steel frame should be improved while the special overload working condition is imitated.

In all special working conditions, the maximum shear stress appeared on the bottom right side of the steel frame on the web in Figure 11. In special overloading condition, the shear stress reaches 67.89 MPa. It is finally burdened by the bolts nearby on the longitudinal connecting plates.

In special overloading conditions, the maximum shear stress is 35.00 MPa after the steel frame is fixed. Compared to the non-welded situation, shear stress reaching 53.55 MPa, that is a 53% decrease. It makes the stress in the whole steel frame more uniform.

4 Test on site

After the completion of hierarchical loading, the propulsion of shield machine is performed. The propulsion progress is divided into the following stages, as shown in the Table 6. In the test on site, the steel-concrete reinforced special segment also has a heavy rotating trend. This segment rotation trend supports the previous rotating characteristic of the steel frame. The diagram of 168 jacks on site is shown in the Figure 14. In order to avoid the damage of the jack, a balance force is applied to this segment and the load on each jack is fine-tuned. The loadings added by 168 jacks under three working conditions according to the Table 6 are listed respectively in Tables 7 to 9.

Figure 14 Jacks on site

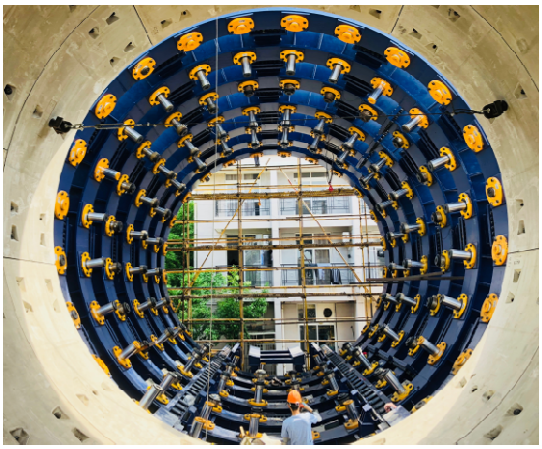

Table 6 Propulsion progress arrangements

No.	*Measuring time*	*Working conditions*
1	2018/5/22 (6:30—7:00)	Before cutting
2	2018/5/22 (10:56—11:00)	To the maximum cutting force (1700 kN)
3	2018/5/22 (21:00—21:20)	Front cutter head cutting through the segment

Table 7 Load on jacks at 7:00 (ton)

Time (7:00)	*1st ring*	*2nd ring*	*3rd ring*	*4th ring*	*5th ring*	*6th ring*	*7th ring*
1	20.90	20.80	26.00	25.90	24.70	20.20	20.00
2	20.60	20.60	25.70	25.50	24.20	19.60	20.00
3	20.10	20.00	24.00	24.00	24.80	19.50	20.00
4	23.40	19.50	25.00	25.00	25.90	22.60	19.00
5	20.00	17.80	25.00	26.00	26.00	18.30	18.00
6	17.20	16.10	21.50	24.00	23.80	15.60	16.00
7	20.70	20.80	26.00	26.00	25.90	20.50	21.00
8	22.60	22.67	28.00	28.00	28.60	22.70	23.00
9	23.60	23.67	29.50	30.00	29.80	23.60	24.00
10	23.60	23.73	29.50	29.80	29.80	23.50	24.00
11	22.70	22.64	28.50	30.00	28.70	22.70	23.00
12	20.70	20.70	26.00	27.00	26.30	20.70	21.00
13	16.60	16.68	21.00	21.50	21.80	18.00	18.00
14	20.80	20.00	23.00	22.50	24.40	17.90	18.00
15	22.50	21.86	25.00	25.00	25.90	19.40	19.00
16	22.10	21.10	25.00	25.00	26.62	18.90	19.00
17	20.90	21.52	27.00	25.00	26.40	18.90	20.00
18	20.00	21.20	26.50	26.50	26.00	21.20	21.00
19	24.70	24.67	31.50	31.50	31.80	24.50	25.00
20	26.50	26.66	34.00	34.00	34.20	26.60	27.00
21	27.70	27.54	35.50	35.50	35.70	27.30	28.00
22	27.70	27.40	35.50	35.50	34.80	27.60	28.00
23	26.50	26.70	34.50	34.50	34.70	26.50	27.00
24	24.80	24.60	31.50	31.50	32.90	24.50	25.00

Table 8 Load on jacks at 11:00 (ton)

Time (11:00)	*1st ring*	*2nd ring*	*3rd ring*	*4th ring*	*5th ring*	*6th ring*	*7th ring*
1	20.86	21.00	26.00	26.00	25.60	19.80	20.00
2	20.60	20.30	26.00	26.00	25.00	21.00	20.00
3	20.20	20.50	25.00	24.00	25.80	21.10	20.00
4	22.90	21.00	25.50	26.00	28.00	22.20	19.00
5	20.20	28.00	24.50	26.00	26.40	20.30	18.00
6	17.10	26.00	21.00	24.00	23.30	15.20	16.00
7	20.66	20.60	25.50	26.00	25.80	20.40	21.00
8	22.60	22.60	28.50	28.10	28.60	22.60	23.00
9	23.50	23.70	29.50	29.70	29.60	23.60	24.00
10	23.50	23.70	29.50	29.50	29.70	23.90	24.00
11	22.60	22.64	28.50	29.00	28.70	23.00	23.00
12	20.65	20.70	25.50	26.00	26.00	20.70	21.00
13	16.60	15.80	21.00	21.50	21.80	18.00	18.00
14	21.00	19.15	24.50	23.50	25.00	18.20	18.00
15	22.75	21.30	26.50	30.10	25.00	19.70	19.00
16	22.00	21.60	26.50	30.50	25.30	18.70	19.00
17	21.00	21.66	27.00	24.50	25.00	19.00	20.00
18	20.68	21.19	26.50	26.00	25.70	20.20	21.00
19	26.79	24.65	30.50	30.50	30.80	24.50	25.00
20	28.50	26.66	33.10	33.50	33.20	26.50	29.00
21	29.70	27.55	34.50	33.50	34.50	26.90	30.00
22	29.60	27.50	34.50	34.00	34.20	27.60	30.00
23	28.50	26.68	33.50	33.00	32.80	26.40	29.00
24	26.70	24.50	31.00	31.00	32.30	24.30	27.00

Table 9 Load on jacks at 21:00 (ton)

Time (21:00)	*1st ring*	*2nd ring*	*3rd ring*	*4th ring*	*5th ring*	*6th ring*	*7th ring*
1	21.00	21.00	27.50	26.50	24.90	19.50	20.00
2	20.50	20.33	26.00	25.00	24.60	19.40	20.00
3	20.36	20.15	24.50	24.50	24.90	19.70	20.00
4	23.80	20.50	25.50	26.00	27.30	21.80	19.00
5	20.60	18.10	24.50	26.00	27.10	18.60	18.00
6	17.20	16.10	22.00	24.00	23.50	15.30	16.00
7	20.70	20.60	26.00	26.00	25.80	20.60	21.00
8	22.60	22.65	28.50	28.50	28.70	24.10	23.00
9	23.50	23.65	29.50	29.50	29.90	23.70	24.00
10	23.60	23.70	29.50	29.50	29.80	23.50	24.00
11	22.72	22.62	28.50	29.50	28.80	22.70	23.00
12	20.65	20.70	25.50	26.00	26.40	20.60	21.00
13	16.77	16.00	21.00	21.30	21.80	18.40	18.00
14	21.40	20.00	24.50	22.90	24.00	18.50	18.00
15	23.20	21.50	26.50	0.03	25.20	20.20	20.00
16	22.40	22.00	27.00	0.00	25.10	19.00	20.00
17	21.25	21.95	27.50	23.00	26.30	19.50	20.00
18	21.10	21.50	27.00	26.50	26.40	20.50	21.00
19	26.65	24.66	30.50	31.00	30.90	24.50	27.00
20	28.62	26.67	33.50	33.30	33.20	24.50	29.00
21	29.72	27.56	34.50	34.30	34.60	26.60	30.00
22	29.50	27.48	34.50	34.30	34.30	27.60	30.00
23	28.45	26.68	33.50	33.30	33.70	26.50	29.00
24	26.55	24.60	30.50	31.00	30.80	24.60	27.00

Measurement points are arranged outside the seven-ring steel frame, as shown in Figure 15. The number of rings is defined as 1st ring to 7th ring from the front to the back of the entire facility, as shown in Figure 15(b). The circumferential stress is measured by strain gage, and the shear stress on the steel frame web is measured by strain rosette. as shown in Figure 15(c). The external deformation of each ring steel structure is monitored by *L*-shaped small prism during the propulsion of shield machine.

The loading amplitude table in Table 7 to 9 is imported into ABAQUS for load setting, and the simulation result data of the area corresponding to the measuring point in Figure 15(a) is extracted. Taking the steel frame of the third ring as the analysis, the test data before cutting (7:00) and finished loading (21:00) are compared with the simulation results, as shown in Figures 16 to 19 and Table 10.

The comparison between the experiment and simulation results shows that:

1) The radial displacement of the steel frame under (7:00) working condition is not consistent with the measured results.

2) The trend of the circumferential displacement of steel frame under (7:00) working condition is consistent with that of the measured one, but the numerical values are inconsistent. The trend of the circular and radial displacements from the simulation results under (21:00) working condition is consistent with the experimental results, but the numerical values are inconsistent.

3) The measured maximum principal stress and Mises stress on the steel frame web are very close to the simulational results, and there is no magnitude difference in the results of maximum shear stress.

Figure 15 Schematic diagram of measuring point layout. (a) Schematic diagram of measuring point layout (b) The definition of the number of rings (c) The strain rosette position (d) The position of the web

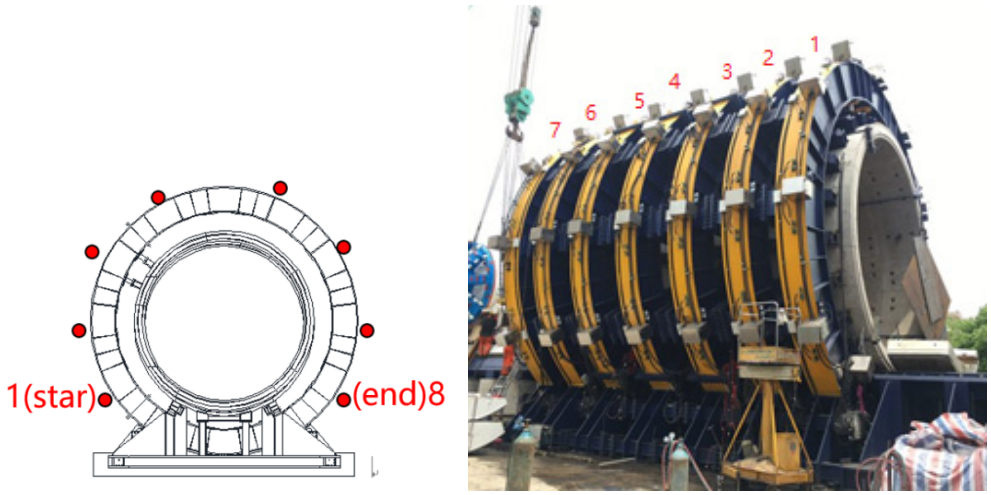

(a) (b)

Figure 15 Schematic diagram of measuring point layout. (a) Schematic diagram of measuring point layout (b) The definition of the number of rings (c) The strain rosette position (d) The position of the web (continued)

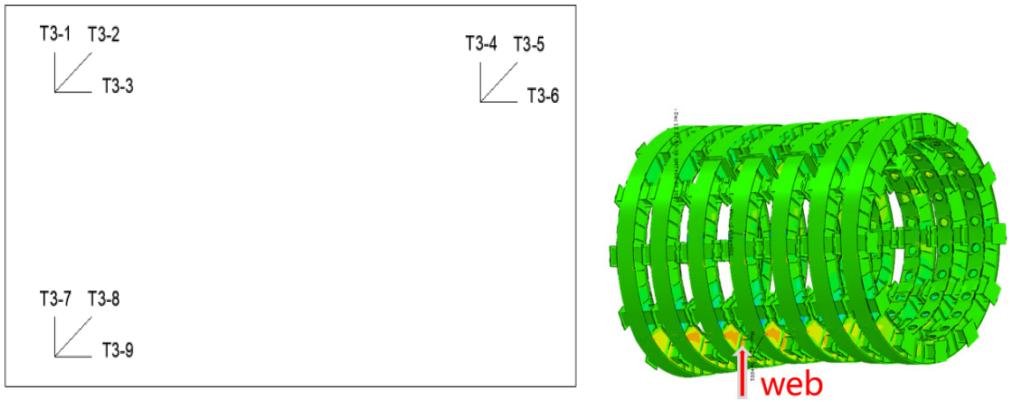

(c) (d)

Figure 16 The comparison of experimental and simulational results about radical displacement (7:00)

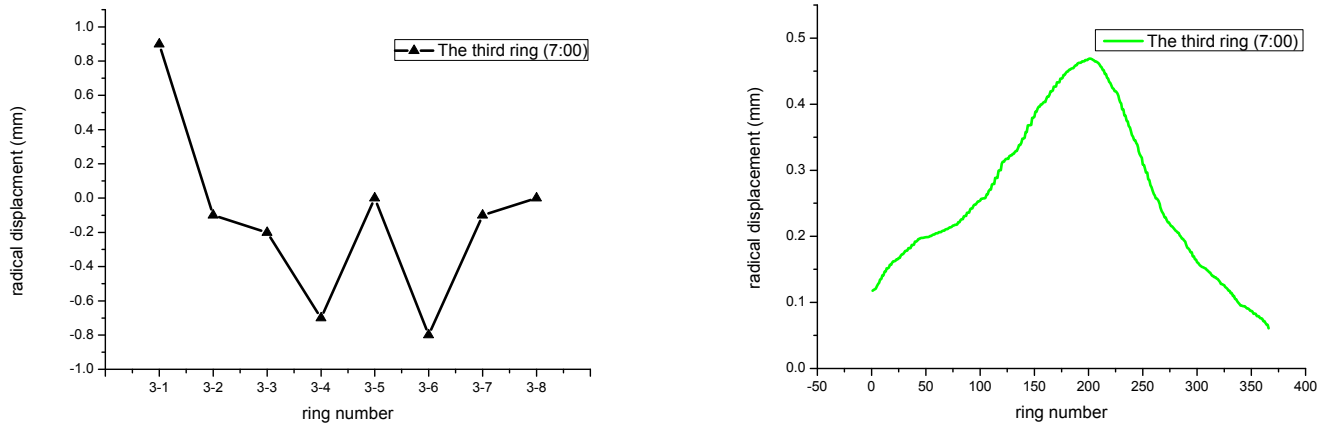

Figure 17 The comparison of experimental and simulational results about circumferential displacement (7:00)

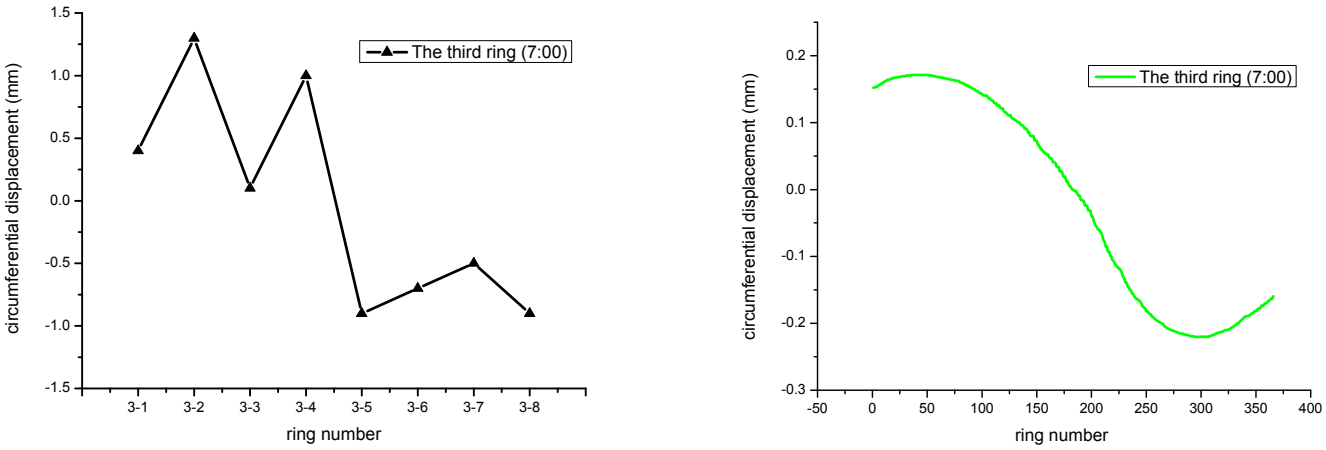

Figure 18 The comparison of experimental and simulational results about radical displacement (21:00)

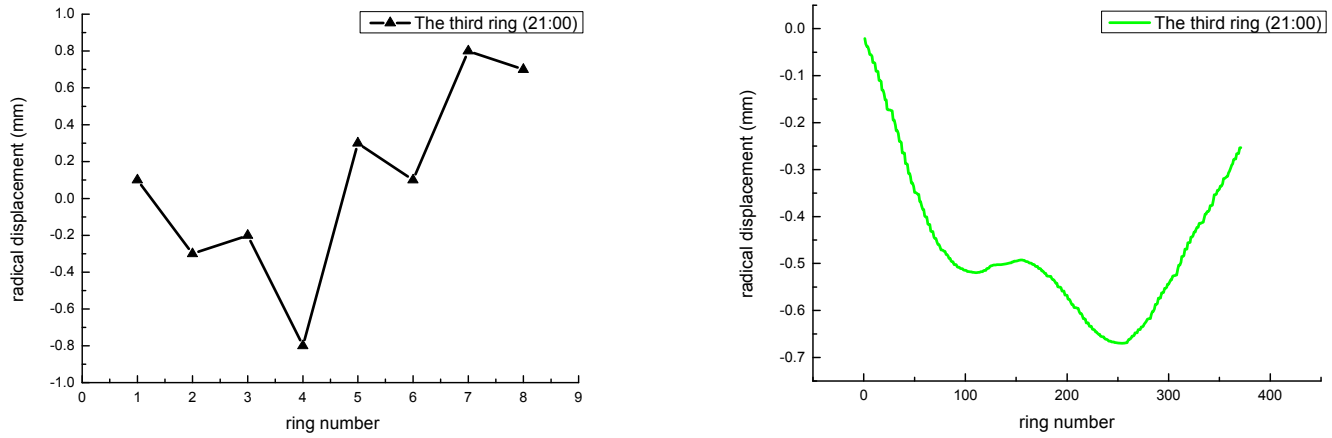

Figure 19 The comparison of experimental and simulational results about circumferential displacement (21:00)

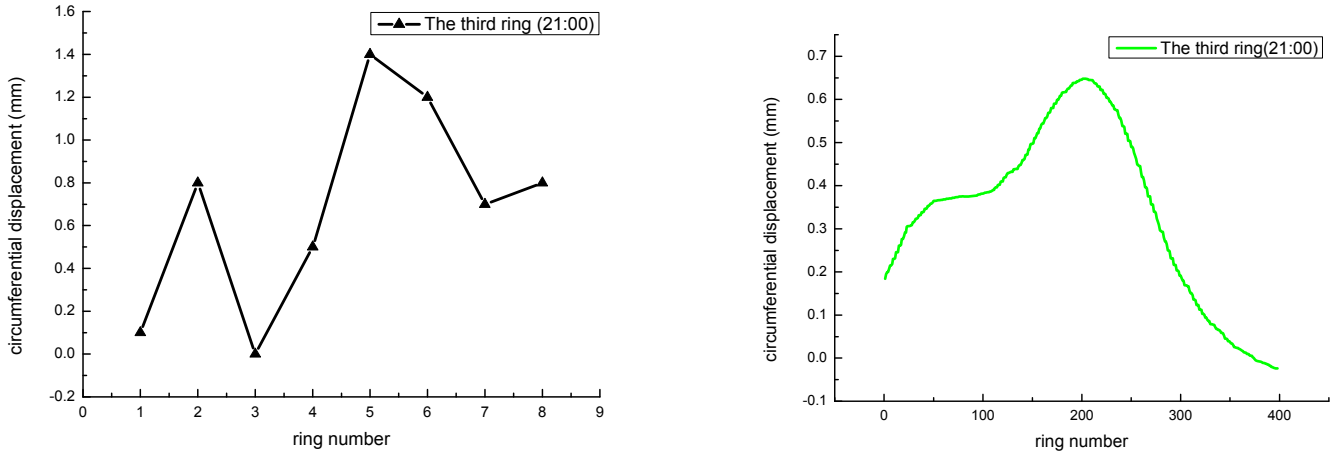

Table 10 The comparison of experimental and simulational results on the web (MPa)

Working conditions	*Simulation*	*Experiment*
	$\sigma_{\text{Mises}} = 16.80$	$\sigma_{\text{Mises}} = 16.62$
	$\sigma_{\text{Mises}} = 16.80$	$\sigma_{\text{Mises}} = 16.43$
	$\tau_{\max} = 4.54$	$\tau_{\max} = 8.03$
Front cutter head cutting through the segment(21:00)	$\sigma_{\text{Mises}} = 20.61$	$\sigma_{\text{Mises}} = 21.21$
	$\sigma_{\text{Mises}} = 24.27$	$\sigma_{\text{Mises}} = 23.72$
	$\tau_{\max} = 5.21$	$\tau_{\max} = 8.57$

5 Conclusions

Through the simulation analysis of the full-scale steel frame model, the following conclusions can be drawn:

1) Simulation results show that when the constraints between the steel frame and foundation base are not taken into account, the steel frame produces a large circumferential displacement. This will directly lead to the damage of the cylinder sliding on the segment during loading, and also directly affect the accuracy of loading. In the subsequent tests, there is indeed a rotational trend, and the results of simulation analysis make the test avoid this risk.

2) The independently controlled cylinder can imitate the real load-displacement curve (the spring effect of the soil) rather than the traditional load eimitation.

3) In various working conditions, the maximum Mises stress occurs on the welded seam or hole inner of the jack installing plate, and the design strength can meet the relevant specification.

4) The design strength of this steel frame under six working conditions meets the simulation requirements. However, for special working conditions, attention should be paid to the circumferential rotation of the facility to avoid the damage of the jack, that is, whether its stiffness is adapted to the requirements.

5) Through the comparison of the experimental measurement results, it is proved that this finite element simulation can provide a certain reference for the structure and avoid some risks during construction and test. At the same time, the feasibility and safety of the structure after welded are also verified.

In summary, when using or installing similar vertical loading facility, it is necessary to weld the steel frame and the foundation to ensure its normal operation in the future.

References

Aso, Y., Yotsuya, T. and Makimoto, A. et al. (1995) 'Mechanical departure and arrival methods for shield tunneling', *J-STAGE*, Vol. 5, pp.231–236. Doi: 10.11532/journalte1991.5.231.

Ding, W.Q., Yue, Z.Q., Tham, L.G., Zhu, H.H., Lee, C.F. and Hashimoto, T. (2004) 'Analysis of shield tunnel', *International Journal for Numerical and Analytical Methods in Geomechanics*, Vol. 28, pp.57–91. Doi: 10.1002/nag.327.

Fang, Y., Wang, H., Guo, J., Chen, Z. and Wu, C. (2016) 'Study on the mechanical behavior and the model test of segmental linings for the shield tunnel undercrossing the yellow river', *Procedia Engineering*, Vol. 166, pp.9–31. Doi: 10.1016/j.proeng.2016.11.532.

GB (2017) *Standard for design of steel structures of the People's Republic of China (GB 50017-2017)*.

Guo, Z., Lu, L. and Liu, Z. (2004) 'Loading method of test for double-circular face shield-tunnel lining', *Structural Engineers*, Vol. 20, pp.64–71. Doi: 10.3969/j.issn.1005-0159.2004.03.014.

Jiwattanakul, J., Youngjitikornkun, C., Kusakunniran, W., Wiratsudakul, A., Thanapongtharm, W. and Leelahapongsathon, K. (2021) 'Map simulation of dogs' behaviour using population density of probabilistic model', *International Journal of Computer Applications in Technology*, Vol. 65, pp.14–24. Doi: 10.1504/IJCAT.2021.113646.

Li, X., Yan, Z., Wang, Z. and Zhu, H. (2015) 'Experimental and analytical study on longitudinal joint opening of concrete segmental lining', *Tunneling and Underground Space Technology*, Vol. 46, pp.52–63. Doi: 10.1016/j.tust.2014.11.002.

Liu, X., Jiang, S. and Liang, X. (2017) *Vertical Loading Test Device for Whole Ring Tunnel Structure*, China Patent, CN106501014A.

Ma, H. (2015) 'Discussion on the loading mode of mechanical properties test of shield segments', *Engineering Construction Standardization*, Vol. 2, pp274–284. (in Chinese)

Sayahi, T., Tatar, A., Rostami, A., Anbaz, M.A. and Shahbazi, K. (2021) 'Determining solubility of CO_2 in aqueous brine systems via hybrid smart strategies', *International Journal of Computer Applications in Technology*, Vol. 65, pp.1–13. Doi: 10.1504/IJCAT.2021.113650.

Zhu, H. (1999) 'Simulation analysis of shield tunnel construction process', *Chinese Journal of Rock Mechanics and Engineering*. (in Chinese)